Published in final edited form as:
Neuron. 2011 June 9; 70(5): 991–1004. doi:10.1016/j.neuron.2011.03.029.

Desynchronization of multivesicular release enhances Purkinje cell output

Stephanie Rudolph[1,2], **Linda Overstreet-Wadiche**[2], and **Jacques I. Wadiche**[2,*]

[1] Department of Biology, University of Freiburg, 79104 Freiburg, Germany

[2] Department of Neurobiology and Evelyn McKnight Brain Institute, University of Alabama at Birmingham; Birmingham, AL 35294 USA

Summary

The release of neurotransmitter-filled vesicles following action potentials occurs with discrete time courses: sub-millisecond phasic release that can be desynchronized by activity followed by 'delayed release' that persists for tens of milliseconds. Delayed release has a well established role in synaptic integration, but it is not clear whether desynchronization of phasic release has physiological consequences. At the climbing fiber to Purkinje cell synapse, the synchronous fusion of multiple vesicles is critical for generating complex spikes. Here we show that stimulation at physiological frequencies drives the temporal dispersion of vesicles undergoing multivesicular release, resulting in a slowing of the EPSC on the millisecond time scale. Remarkably, these changes in EPSC kinetics robustly alter the Purkinje cell complex spike in a manner that promotes axonal propagation of individual spikelets. Thus, desynchronization of multivesicular release enhances the precise and efficient information transfer by complex spikes.

Keywords

synaptic transmission; Purkinje cell; climbing fiber; vesicle fusion

Introduction

The well-established role of timing in neural computation has resulted in detailed knowledge of the mechanisms that enable precise control of neural signaling on the millisecond timescale, from the level of single proteins to entire circuits. For example, the release of neurotransmitter vesicles following an action potential is not instantaneous but rather dispersed in time (Katz and Miledi, 1965a, b). In hippocampal neurons, the decay of the vesicle release rate matches closely to the decay phase of EPSCs, suggesting that release asynchrony is the major determinant of the time course of evoked synaptic currents (Diamond and Jahr, 1995). Additionally, prolonged phases of asynchronous release that persist for tens and hundreds of milliseconds, termed *delayed release*, can also occur at some excitatory and inhibitory synapses (e.g. Atluri and Regehr, 1998; Lu and Trussell, 2000; Hefft and Jonas, 2005) with profound consequences for synaptic integration

*Correspondence should be addressed to: Jacques I. Wadiche, Department of Neurobiology, SHEL 1005, University of Alabama at Birmingham, Birmingham, AL 35294, Phone: 205-996-6413, jwadiche@uab.edu.

(Iremonger and Bains, 2007; Crowley et al., 2009). Desynchronization of phasic release that occurs on the millisecond time scale may account for the kinetic differences reported in release latency or postsynaptic responses (Waldeck et al., 2000; Wadiche and Jahr, 2001; Scheuss et al., 2007), but little is known about the physiological significance of synaptic timing cues on this scale (Boudkkazi et al., 2007).

The fusion of multiple vesicles and subsequent neurotransmitter release from a single active site is known as multivesicular release (MVR; Tong and Jahr, 1994; Auger et al., 1998; Prange and Murphy, 1999; Wadiche and Jahr, 2001; Oertner et al., 2002; Biró et al., 2006; Christie and Jahr, 2006). At climbing fiber to Purkinje cell (CF-PC) synapses, low frequency stimulation generates synchronized MVR that drives a high glutamate concentration within the synaptic cleft (Wadiche and Jahr, 2001). However, since CFs fire at a rate of 1 – 2 Hz *in vivo* (Armstrong and Rawson, 1979; Campbell and Hesslow, 1986), here we test the effects of stimulation frequency on the time course of PC responses. We find that physiologically-relevant stimulation frequencies desynchronize MVR leading to EPSCs with slower kinetics that are sufficient to alter the spike waveform of PCs, the sole output of the cerebellum. Paradoxically, activity-dependent desynchronization enhances the fidelity of information carried by the distinctive high-frequency burst of spikes known as the complex spike. Together, these data suggest that regulation of synaptic timing by desynchronization of phasic vesicle release may be a mechanism for refining temporal signaling in the CNS.

Results

Frequency-dependent decrease in EPSC amplitude is accompanied by kinetic changes

We studied synaptic transmission in Purkinje cells (PCs) from acute cerebellar slices. Climbing fiber (CF) stimulation at 0.05 Hz generated large, all-or-none AMPA receptor (AMPAR)-mediated EPSCs with little fluctuation in peak amplitude or kinetics (Figure 1A and 1B1). Stimulation at 2 Hz, similar to the average firing frequency of CFs *in vivo* (Armstrong and Rawson, 1979; Campbell and Hesslow, 1986), caused a time-dependent decrease of the EPSC amplitude that stabilized after 100 – 150 pulses (Figure 1A; also see Dittman and Regehr, 1998; Foster and Regehr, 2004). On average, the amplitude of EPSCs evoked during 2 Hz stimulation ($EPSC_{2Hz}$) was reduced by 29.5 ± 2.3% compared to that at 0.05 Hz ($EPSC_{0.05Hz}$; Figure 1C1; n = 30). At CF synapses, high frequency-dependent reduction in the EPSC amplitude is thought to result from depletion of neurotransmitter-filled vesicles(Zucker and Regehr, 2002; Foster and Regehr, 2004). These results confirm that vesicle depletion also occurs at physiologically relevant stimulation frequencies (Dittman and Regehr, 1998; Foster and Regehr, 2004).

Interestingly, repetitive stimulation at 2 Hz also caused a gradual slowing of the EPSC kinetics (Figure 1B2). The EPSC rise times (20–80%) increased from 0.42 ± 0.02 ms at 0.05 Hz stimulation to 0.59 ± 0.03 ms at 2 Hz stimulation (Figure 1C2; $p < 0.0001$; n = 30) and the decay times increased from 4.5 ± 0.2 ms at 0.05 Hz to 5.3 ± 0.4 ms at 2 Hz (Figure 1C3; n = 30; $p < 0.0001$). Importantly, these kinetic changes partially conserved the charge of each EPSC. The current-time integral decreased by 20.4 ± 2.6%, significantly less than the reduction of the amplitude during 2 Hz stimulation (29.5 ± 2.3%; n = 30; $p < 0.001$). The additional charge that occurs as a result of EPSC kinetic slowing affects PC output (see below).

The peak EPSC amplitude did not correlate with the rise or decay kinetics (Figure 1D), arguing that the EPSC kinetics did not result from dendritic filtering or inadequate voltage clamp. Nevertheless, we tested whether the EPSC amplitude influenced its kinetics by including a sub-saturating concentration of the high-affinity AMPAR antagonist, NBQX (600 – 800 nM) or recording at depolarized membrane potentials. Neither of these

manipulations affected the results and the data was pooled for analysis (Figure 1; n = 14 and 16, respectively). Additionally, we monitored the series resistance (R_s) during each experiment and rejected experiments when the R_s was unstable. On average, R_s during $EPSC_{2Hz}$ was 102 ± 5.7 % of the value during $EPSC_{0.05Hz}$ stimulation (average 2.7 ± 1.4 MΩ; range 1.5 – 4.9 MΩ; n = 30; p > 0.05). We also considered whether dendritic filtering contributed to the EPSC kinetic slowing. However, there was no correlation between the EPSC rise and decay times as expected if these parameters were significantly filtered by the dendritic cable (data not shown; p = 0.98 Hestrin et al., 1990). Together this suggests that changes in voltage control or in dendritic filtering do not contribute to the kinetic slowing that occurs with increased stimulation frequency.

Slowing of the EPSC time course occurred across a range of physiologically-relevant frequencies. Although increasing the stimulus frequency to 0.2 Hz had no effect on the EPSC kinetics, further increase to 1, 2 and 4 Hz caused significant prolongation of both the rise and decay times (Figure S1A; n = 4 – 9; p < 0.05). Increasing the stimulation frequency to 10 Hz did not further slow the EPSC (data not shown), suggesting that at higher frequencies vesicular depletion may outweigh desynchronization. We also tested whether EPSC slowing requires prolonged repetitive stimulation. The rise time of the third EPSC during a brief 15 Hz train was slower than that of the first EPSC (Figure S1B; 0.62 ± 0.1 ms and 0.41 ± 0.05 ms, respectively; n = 11; p < 0.001) and similar kinetic differences were found when CFs were stimulated with two pulses at 20 Hz (n = 15, not shown). Thus, activity-dependent slowing of EPSCs occurs across physiologically-relevant stimulation paradigms.

We posit that increasing CF stimulation frequency not only leads to the depletion of the available vesicles *but also* desynchronizes the timing of vesicle fusion leading to EPSCs that are smaller in amplitude with slower kinetics. Whereas activity-dependent vesicle depletion reduces the EPSC amplitude, release desynchrony shapes the EPSC time course.

Kinetic changes require multivesicular release

Action potentials trigger well-timed phasic vesicle fusion (synchronous release) that is sometimes followed by a smaller elevation in quantal release called ‘delayed’ or ‘asynchronous release’ that lasts for tens of milliseconds (Barrett and Stevens, 1972; Goda and Stevens, 1994; Isaacson and Walmsley, 1995; Atluri and Regehr, 1998). Asynchronous release presumably results from jitter in the timing of vesicle fusion between synapses, or *inter-site* asynchrony. However, MVR introduces the additional possibility of vesicle release desynchronization *within* each release site. To test whether frequency-dependent depression in EPSC peak amplitude and accompanying kinetic changes require MVR, we lowered extracellular Ca^{2+} to promote the fusion of, *at most*, one vesicle per release site, or univesicular release (UVR). Under these conditions, the amplitude of EPSCs was 68.5 ± 3.4% (n = 6) smaller. Increasing CF stimulation frequency from 0.05 Hz to 2 Hz caused a similar reduction of the EPSC peak amplitude and its current-time integral (40.0 ± 3.0% and 36.0 ± 2.9% decrease, respectively; Figure 2; n = 18; p > 0.05) because there was no change in the EPSC kinetics. Neither the EPSC rise (0.42 ± 0.02 and 0.44 ± 0.02 ms; p > 0.05) nor decay (2.6 ± 0.2 and 2.6 ± 0.2 ms; p > 0.05) were altered by increasing the stimulation frequency from 0.05 to 2 Hz (Figure 2B and 2C). These results suggest that activity-dependent slowing of EPSC kinetics requires MVR since it is not present under conditions of UVR.

We also recorded EPSCs in an extracellular solution that more closely approximates the$[Ca^{2+}]$ *in vivo* (Borst, 2010). The peak EPSC amplitude was reduced by 43.3 ± 5.6% when the extracellular $[Ca^{2+}]$ was lowered from 2.5 to 1 mM (n = 7). Increasing the stimulation frequency from 0.05 Hz to 2 Hz slowed the EPSC rise time from 0.37 ± 0.02 ms

to 0.46 ± 0.05 ms (n = 7; $p < 0.01$) suggesting that MVR desynchronization persists in an extracellular [Ca^{2+}] solution similar to *in vivo* conditions.

Because extracellular [Ca^{2+}] can contribute to the presynaptic action potential waveform (Schneggenburger et al., 1999), we also reduced MVR through activation of metabotropic glutamate receptors (mGluRs) that suppress transmitter release (Takahashi et al., 1996). The mGluR agonist L-CCG-I (20 μM), reduced the peak EPSC amplitude by 50.6 ± 5.7% (n = 7), qualitatively similar to lowering extracellular Ca^{2+} to 0.5 mM, where UVR predominates. In L-CCG-I, increasing CF stimulation frequency from 0.05 Hz to 2 Hz no longer slowed the EPSC rise or decay (n = 7; $p > 0.05$; ANOVA), further suggesting that activity-dependent kinetic changes requires MVR. The lack of kinetic changes under conditions of UVR supports the notion that desynchronization of multiple vesicles released *within* each release site, or *intra-site* vesicle desynchronization, underlies EPSC kinetic slowing.

Lower peak synaptic glutamate concentration with increased stimulation frequency

Vesicle depletion predicts that during UVR, when transmission is constrained to the release of zero or one vesicle with each action potential, frequency-dependent synaptic depression is due to fewer active sites. With this limitation, the synaptic glutamate transient will not be altered during depression. We tested this idea by monitoring the inhibition of EPSCs with a low-affinity AMPAR antagonist, kynurenic acid (KYN). In 0.5 mM Ca^{2+}, KYN (1 mM) inhibited EPSCs to the same degree at both 0.05 and 2 Hz (83.3 ± 1.2% and 87.2 ± 6.6% inhibition, respectively; Figure 3A and 3B; n = 7; $p > 0.05$). Thus, under conditions of UVR, the decrease of the EPSC peak amplitude during 2 Hz stimulation results from a reduction in the number of active sites without a change in the synaptic glutamate concentration.

Conversely, depression under conditions of MVR can result from a lower glutamate concentration due to fewer vesicles released per site in addition to a reduction in the number of active sites. Indeed, in 2.5 mM Ca^{2+}, the magnitude of KYN inhibition was activity-dependent: $EPSC_{0.05Hz}$ was inhibited to a lesser degree than $EPSC_{2Hz}$ (42.4 ± 3.1% versus 65.0 ± 2.2%, respectively; Figure 3C and 3D; n = 16, $p < 0.0001$). This suggests that synaptic AMPARs sense a glutamate concentration that is smaller during 2 Hz compared to 0.05 Hz stimulation yet larger than in 0.5 mM Ca^{2+}.

In the same cells, we also tested the effects of a low dose of NBQX. Inhibition by NBQX will only depend on the concentration of the antagonist. NBQX (100 nM) inhibition at 0.05 Hz and 2 Hz was not significantly different in 0.5 mM Ca^{2+} (36.4 ± 2.7% and 36.8 ± 2.4% block, respectively, n = 7) from that in 2.5 mM Ca^{2+} (44.6 ± 4.4% and 45.3 ± 4.6% block, respectively; Figure 3; n = 16; $p > 0.05$; ANOVA). Because the actions of NBQX do not depend on extracellular Ca^{2+} or stimulation frequency, we conclude that the differential inhibition observed with KYN is not a result of poor voltage control. Together these data argue that *both* vesicle depletion and MVR desynchronization act to lower the synaptic concentration gradient during repetitive stimulation: while depletion predicts that fewer vesicles are released at each site, desynchrony causes temporal dispersion of the synaptic concentration transient.

Lower synaptic glutamate during Sr^{2+}- evoked asynchronous release

At MVR synapses, the simplest mechanism that accounts for a decrease in the synaptic glutamate concentration is the release of fewer vesicles at each active zone. To determine whether release desynchronization also lowers the synaptic glutamate transient, we tested the EPSC sensitivity to KYN in the presence of the divalent cation strontium (Sr^{2+}). Strontium is routinely used to increase ‘delayed release’ and isolate quantal events

underlying phasic release (for example see Goda and Stevens, 1994; and Figure 5) but can also support phasic release with lower efficiency and more desynchrony than calcium (Xu-Friedman and Regehr, 2000). We mimicked the amplitude and kinetic effects of 2 Hz stimulation by titrating the extracellular recording solution with increasing concentrations of Sr^{2+}. Replacing Ca^{2+} with 5 mM strontium resulted in 0.05 Hz-evoked EPSCs ($ESPC_{Sr2+}$) that were 23.7 ± 8.4% smaller and slower than in Ca^{2+} (Figure 4A and 4B; n = 9, $p < 0.01$). Using this Sr^{2+}-based extracellular solution and continuing to stimulate CFs at a frequency of 0.05 Hz, we addressed whether desynchronization of phasic release is sufficient to reduce the synaptic glutamate concentration by comparing the KYN inhibition of EPSCs recorded in Sr^{2+} to that with Ca^{2+}. The KYN inhibition of the peak EPSC amplitude in Sr^{2+} was greater than in a Ca^{2+}-based solution (Figure 4C and 4D; 58.1 ± 1.9% and 41.2 ± 1.8% block, respectively, n = 9, $p < 0.01$). These results suggest that desynchronization of phasic release can mimic the alterations of EPSC kinetics and the lower synaptic glutamate concentration that occurs with 2 Hz CF stimulation.

Quantal amplitude does not change during increased activity

An alternative possibility to desynchronization is that increased stimulation frequency decreases vesicular neurotransmitter content or changes in vesicle pore dynamics (Choi et al., 2000). To estimate changes in the size and kinetics of single vesicle fusion, we recorded asynchronous quantal-like events evoked by CF-stimulation in the presence of 0.5 mM Sr^{2+}. The amplitude of averaged asynchronous EPSCs (aEPSCs; Figure 5A) was not different with 2 Hz or 0.05 Hz CF stimulation ($aEPSC_{2Hz}$ was 102.7 ± 3.6% of $aEPSC_{0.05Hz}$; n = 11; $p > 0.05$). A comparison of the cumulative probability histograms of both frequencies shows that there was no significant difference in the aEPSC amplitude distributions (Figure 5B). Importantly, the rise and decay kinetics of aEPSCs at 0.05 and 2 Hz were similar (n = 11; $p > 0.05$). These results indicate that the kinetics and the size of quantal AMPAR-mediated responses are unchanged during 2 Hz stimulation, thus the EPSC kinetic changes are not due to a decrease in quantal size or altered dynamics of vesicle fusion.

Glutamate pooling or AMPA receptor desensitization do not account for EPSC slowing

Although Bergmann glia and PCs express glutamate transporters that limit the extracellular glutamate concentration, repetitive CF stimulation can lead to transmitter spillover onto nearby synapses and activation of extrasynaptic AMPARs (Tzingounis and Wadiche, 2007). Inhibition of glutamate transporters by TBOA (50 μM) slowed the decay of $EPSC_{0.05Hz}$ (n = 9, $p < 0.001$) without affecting the rise time (Figure 5C – 5E; n = 9; $p > 0.05$) or $EPSC_{0.05Hz}$ peak amplitude (96.1 ± 4.8% in TBOA compared to control; n = 9; $p > 0.05$). We interpret these results to mean that inhibition of glutamate uptake predominantly amplifies the response due to transmitter spillover to extrasynaptic receptors that occurs following near-synchronous MVR (Wadiche and Jahr, 2001).

In contrast, neither the kinetics nor the amplitude of $EPSC_{2Hz}$ were altered by TBOA application (Figure 5C – E; $p > 0.05$; ANOVA). This implies that the synaptic glutamate transient during 2 Hz CF-stimulation is brief and does not activate extrasynaptic AMPA receptors. Alternatively, repetitive stimulation at low stimulation frequencies could cause transmitter pooling and transporters to be overwhelmed, thus occluding TBOA's effects. But several pieces of data argue against this possibility. First, 2 Hz stimulation results in a smaller peak glutamate concentration that likely represents a reduction in the number of vesicles released per site, thus reducing any effects of transmitter pooling due to MVR. Second, the time course of the $EPSC_{0.05Hz}$ decay in the presence of TBOA is significantly slower than the $EPSC_{2Hz}$ decay with uptake intact (Figure 5E; 6.1 ± 0.4 ms and 4.9 ± 0.4 ms; n = 9, $p < 0.05$; ANOVA), arguing against occlusion. Third, inhibition by the low-affinity antagonist (γ-D-glutamyl-glycine) is unaffected by TBOA application suggesting

that transmitter spillover or pooling does not contribute to the fastest components of the synaptic glutamate transient (Wadiche and Jahr, 2001; DiGregorio et al., 2002). Lastly, 2 Hz CF stimulation decreases the EPSC amplitude and slows both its rise and decay, while TBOA application only slows the EPSC decay. Together, these data strongly suggest that the slowing of the $EPSC_{2Hz}$ kinetics occurs through a mechanism separate from transmitter pooling following glutamate uptake inhibition.

Our data suggests that a presynaptic locus is responsible for the activity-dependent EPSC changes. However, postsynaptic mechanisms, such as slow recovery from receptor desensitization and/or occupancy, have been shown to confound the interpretation of ostensibly presynaptic effects (Harrison and Jahr, 2003; Xu-Friedman and Regehr, 2003). Thus, we recorded $EPSC_{0.05Hz}$ and $EPSC_{2Hz}$ in the presence of cyclothiazide (CTZ; 100 μM) to relieve receptor desensitization. As in control conditions, 2 Hz stimulation reduced the peak EPSC amplitude (39.7 ± 8.7%; n = 6) and current-time integral (28.2 ± 9.0%; n = 6). CTZ slowed the 0.05 Hz-evoked EPSC compared to conditions when receptor desensitization was intact, yet the EPSC was further slowed by 2 Hz stimulation (rise time = 0.77 ± 0.07 vs 1.06 ± 0.13 ms and decay time 9.5 ± 1.0 vs 11.7 ± 0.9 ms at 0.05 Hz vs 2 Hz, respectively; n = 6 for each; $p < 0.05$). To rule out a potential confound of postsynaptic receptor saturation, we also recorded CF-PC EPSCs in the continuous presence of KYN (1 mM). The frequency-dependent slowing of the EPSC rise time (0.31 ± 0.01 ms and 0.53 ± 0.07 ms, n = 5; $p = 0.01$) and decay time (2.9 ± 0.2 ms and 3.4 ± 0.3 ms, n = 5; $p < 0.05$) still persisted. These results indicate that postsynaptic receptor desensitization and/or saturation do not play a role in the activity-dependent slowing of the EPSC kinetics. Altogether these data are consistent with a mechanism whereby the $EPSC_{2Hz}$ kinetics are shaped by individual brief transmitter concentration transients that are temporally dispersed during desynchronized MVR (see Figure 9).

Frequency-dependent attenuation of CF-evoked spikelets

We wondered whether activity-dependent changes in the EPSC produced by MVR desynchronization affects PC output. The voltage response triggered by CF stimulation, the complex spike (CpS), consists of bursts of several spikelets (Figure 6A). The shape of the CpS waveform influences spikelet propagation and likely the amount of transmitter released to target neurons (Khaliq and Raman, 2005; Monsivais et al., 2005). Although the CpS waveform is highly reproducible within individual PCs, its kinetics vary considerably between PCs (Schmolesky et al., 2002; Davie et al., 2008) and is sensitive to activity-dependent changes (Hashimoto and Kano, 1998; Maruta et al., 2007). Indeed, we found that the number of spikelets varied across physiologically-relevant CF stimulation frequencies (Figure S2) paralleling the effects seen with the EPSC (Figure S1). CpSs evoked by 2 Hz CF stimulation had fewer spikelets compared to those recorded during 0.05 Hz stimulation (Figure 6A and 6B; 2.8 ± 0.14 and 3.7 ± 0.12, respectively; n = 26; $p < 0.0001$). Individual spikelets were also altered during 2 Hz stimulation in an unexpected manner (Figure 6C – 6E). While the amplitude of the first spike was not different, the second and third spikelet amplitude increased with 2 Hz stimulation relative to the corresponding spikes at 0.05 Hz (by 1.5 ± 1.3%, 33.4 ± 7.3%; 62.2 ± 16.8%, respectively; n = 26, 26, and 18; $p > 0.05$, $p < 0.0001$, and $p < 0.01$, one sample t-test). Similarly, the rate of rise for all spikelets during 2 Hz stimulation differed from the corresponding spikelets at 0.05 Hz (−8.2 ± 2.0%, 68.5 ± 32.2%, 54.7 ± 13.9%, respectively; n = 26, 26, and 18; $p < 0.001$ each; one sample t-test). Lastly, the interspike interval (ISI) between the first and the second pair of spikelets was prolonged during 2 Hz stimulation (27.2 ± 4.2% and 23.1 ± 4.6%; n = 26 and 18; $p < 0.001$ each; one sample t-test). Since increases in spike height, rising rate and ISI are positively correlated with reliability of spikelet propagation in PC axons (Khaliq and Raman, 2005;

Monsivais et al., 2005), this implies that frequency-dependent changes in the CpS waveform promote more efficient spikelet propagation to PC target neurons.

We wondered whether the reduction in the synaptic charge that occurs with 2 Hz stimulation (Figure 1A) was sufficient to account for the activity dependent changes in CpS waveform. To test this possibility, we used NBQX to reduce the EPSC charge to a similar degree as 2 Hz stimulation. This strategy allowed us to distinguish the contribution of amplitude versus kinetics to the CpS waveform because, even at high concentrations, NBQX application has no effect on the EPSC current time course (Figure S3). At 100 nM, NBQX inhibited the EPSC peak amplitude by ~ 30% (Figure 6F, similar to Figure 3; unpaired t-test; $p > 0.05$), resulting in a reduction of the current-time integral of 30.0 ± 2.8% ($n = 4$) that is equivalent to the depression of the EPSC peak amplitude (~ 30%) and significantly more than the decrease of the current-time integral (~ 20%) caused by 2 Hz stimulation (Figure 1). However, application of 100 nM NBQX had no significant effect on the CpS evoked by 0.05 Hz stimulation (Figure 6G – 6K). As expected, further inhibition of AMPARs with higher concentrations of NBQX (300 nM) reduced the number of spikelets (from 3.6 ± 0.4 to 2.4 ± 0.2; $n = 5$; $p < 0.05$) within each CpS (data not shown; see also Foster et al., 2002). These intriguing results indicate that inhibition of AMPAR peak amplitude to a similar degree as during 2 Hz stimulation is not sufficient to alter the CpS waveform but rather suggests that the EPSC kinetics may play a significant role in shaping PC output.

Kinetics of somatic current injection regulate CpS-like responses

We next tested whether the kinetics of somatic current injections can affect the CpS waveform. By adjusting the amplitude of the somatic current injection (range: 5 – 18 nA), we triggered complex-like spikes (Cp-like-Ss) that closely resembled synaptically-stimulated CpSs (Figure 7; McKay et al., 2005; Davie et al., 2008). First, we injected a current (I_{fast}; Figure 7A; 0.4 ms rise and 4 ms decay) that triggered a Cp-like-S with the maximal number of spikelets without inactivation that occurs with increasing current injection (Davie et al., 2008). Repetitive 2 Hz injection of I_{fast} did not alter any parameter of Cp-like-Ss, suggesting that 2 Hz stimulation does not alter CpSs simply by inactivation of voltage-gated conductances (Figure S4). We then reduced the amplitude of the injected current by 20% without altering the kinetics ($I_{fast\text{-}20\%Q}$; Figure 7A). This value matches the reduction of the current-time integral that occurs with 2 Hz synaptic stimulation (Figure 1; charge is reduced by 20.4 ± 2.6%). Decreasing the amplitude (and charge) by 20% did not alter the number of spikelets (Figure 7B; $n = 6$; $p > 0.05$; ANOVA), although there was a slight reduction in the amplitude of the first spikelet (Figure 7C and 7D; $n = 6$). With further reduction of the somatically-injected charge (30% of I_{fast}) the number of spikelets decreased (Figure S5; $n = 6$; $p < 0.05$; ANOVA). Finally, we imposed the same charge as $I_{fast\text{-}20\%Q}$ but with altered kinetics by decreasing the injected current peak amplitude and slowing the decay time to 5 ms. The resulting current waveform ($I_{slow\text{-}20\%Q}$; Figure 7A) had a peak amplitude and a current-time integral that was reduced by 36% and 20%, respectively, compared to I_{fast}. The number of spikelets evoked by $I_{slow\text{-}20\%Q}$ was reduced compared to those evoked by I_{fast} (Figure 7B; 2.8 ± 0.17 and 4.2 ± 0.3; $n = 6$; $p < 0.05$; ANOVA). This suggests that the quantity of somatic charge is not the sole determinant of the number of spikelets and that the kinetics of the injected current can regulate the shape of the Cp-like-S waveform. Remarkably, the $I_{slow\text{-}20\%Q}$ waveform altered the spike height, rising rate, and ISI of the Cp-like-S response in the same manner as 2 Hz synaptic stimulation affected the CpS (compare Figures 6C – E and 7C – E). For the second and third spikelet, the increase in spike height (69.3 ± 23.5% and 166.5 ± 68.0%; $n = 6$ and 5; $p < 0.05$; ANOVA), rate of rise (80.4 ± 43.1% and 101.9 ± 37.8%; $n = 6$ and 5; $p < 0.05$; ANOVA), and ISI (22.2 ± 7.7% and 30.8 ± 10.1%; $n = 6$ and 5; $p < 0.05$; ANOVA) caused by $I_{slow\text{-}20\%Q}$ is predicted to increase the reliability of spikelet propagation. The decrease in the first spikelet height

(−18.8 ± 2.4%; n = 6; $p < 0.05$; ANOVA) and its rate of rise (−23.0 ± 4.7%; n = 6; $p < 0.05$; ANOVA) is unlikely to affect propagation because it is already highly reliable (Khaliq and Raman, 2005; Monsivais et al., 2005). Thus, although there are fewer spikelets with the injection of $I_{slow\text{-}20\%Q}$ or by 2 Hz synaptic stimulation, each spikelet is likely to have a greater chance for propagation.

Activity-dependent propagation of complex spikes

To directly determine whether increased activity and accompanying changes in the CpS waveform affect axonal propagation of spikelets, we stimulated CFs and recorded simultaneously from the soma and axon (Figure 8A). The axonal recording sites were approximately 200 μm from the soma which is distal to the spike initiation site (Clark et al., 2005). Consistent with the measures from somatic CpSs, the first spike successfully propagated regardless of the stimulation frequency. Increasing the stimulation frequency from 0.05 to 2 Hz resulted in fewer somatic spikes that were, on average, more efficiently propagated down to the axonal recording site. After determining whether somatic spikelets successfully propagated to the axonal recording site (see Experimental Procedures), we calculated the cumulative propagation probability of '*x*' number of spikelets regardless of position within the CpS. In recordings shown in Figure 8B, the cumulative probability of having *at least* 2 or 3 spikes successfully propagate down the axon is 0.5 and 0, respectively, although the somatic recording always has three spikelets. At 2 Hz, the cumulative probability of *at least* 2 spikelets propagating increases to 1, equal to the propagation probability for 1 spikelet and matching the number of somatic spikelets. On average, the propagation probability of *at least* 2 and *at least* 3 spikelets increased from 0.61 ± 0.1 and 0.24 ± 0.06 at 0.05 Hz to 0.87 ± 0.05 and 0.52 ± 0.14 at 2 Hz, respectively (Figure 8C, n = 10 dual somatic and axonal recordings; $p < 0.05$). Thus we conclude that desynchronization of MVR enhances the information transfer by CpSs.

Discussion

We show that stimulation of CFs across physiological frequencies results in desynchronization of vesicle fusion as summarized in Figure 9. Synchronized univesicular release (UVR; Figure 9A1) results in a low synaptic glutamate concentration transient (Figure 9B1) that likely mediates complex spikes (CpSs) that resemble simple spikes (Figure 9C1). Multivesicular release (MVR; Figure 9A2) leads to a high synaptic glutamate concentration that is prolonged (Figure 9B2) and CpSs with several spikelets on top of an after-depolarization (Figure 9C2). Increased activity desynchronizes MVR (desync. MVR; Figure 9A3) with reduced but prolonged synaptic glutamate transients (Figure 9B3) that decrease the number of spikelets within each CpS (Figure 9C3) but enhances axonal propagation. This desynchronization disrupts the timing of MVR at individual active zones and occurs concomitantly with vesicle depletion. Desynchronized MVR causes a slowing of the EPSC that preserves a portion of the charge transfer through PC AMPARs. As a consequence, the properties of spikelets that make up CpS are altered in a manner that promotes reliable propagation of individual spikelets. Together these results illustrate how apparently subtle alterations in the timing of MVR control PC output.

A continuum of transmitter release

Measurements of the latency fluctuations of evoked neurotransmitter release, together with the observation that the time course of individual quanta and the EPSC are similar, led to the idea that most transmitter release is highly synchronized (Katz and Miledi, 1965a). Yet, the release process is a temporal continuum of three components: 1) synchronous phasic transmitter release tightly timed to presynaptic stimulation, 2) an intermediate phase that represents desynchronization of the fast release mode on the millisecond timescale

(described here), and 3) an asynchronous release mode that persists for tens to hundreds of milliseconds, often referred to as 'delayed release.' Varied contribution of each release component enables a wide heterogeneity of temporal release patterns across excitatory and inhibitory synapses.

At low frequency stimulation of CF-PC synapses, the timing of vesicle fusion is highly synchronous with essentially no contribution of desynchronized or delayed release (Wadiche and Jahr, 2001). The frequency dependent desynchronization we describe appears similar to the activity-induced prolongation of the phasic vesicle release rate at the calyx of Held (Fedchyshyn and Wang, 2007; Scheuss et al., 2007), hippocampus (Diamond and Jahr, 1995), cortex (Boudkkazi et al., 2007), and other synapses (Auger et al., 1998; Vyshedskiy et al., 2000; Waldeck et al., 2000). Yet activity-dependent desynchronization at CF synapses does not recruit delayed release, as described at other synapses following repetitive activation (Atluri and Regehr, 1998; Lu and Trussell, 2000; Hefft and Jonas, 2005; Iremonger and Bains, 2007). These observations suggest that rapid activity-dependent conversion between synchronous and desynchronized release modes represents different states of the same release machinery, whereas delayed release may require distinctive release proteins (Sun et al., 2007).

Physiological consequences of release timing

Previous work has identified a prominent role for delayed release in regulating spike integration (Lu and Trussell, 2000; Hefft and Jonas, 2005; Iremonger and Bains, 2007). A contribution of delayed release to integration makes sense considering the time course of delayed release can be longer than the time constant of most neurons. It is harder, however, to predict the significance of desynchronized vesicle release on the millisecond timescale. This may explain why the physiological consequences of desynchronized release have remained largely unexplored, despite the demonstration that this form of release occurs throughout the brain (Diamond and Jahr, 1995; Auger et al., 1998; Vyshedskiy et al., 2000; Waldeck et al., 2000; Fedchyshyn and Wang, 2007; Scheuss et al., 2007). It is proposed that regulation of release latency on the millisecond timescale provides a temporal code that may enrich the storage capacity of neural networks (Boudkkazi et al., 2007). Although the mechanisms that enable the CpS to respond to millisecond alterations in the EPSC are not clear, our results demonstrate that PCs can also integrate activity-dependent changes on this time scale.

Mechanisms of activity-dependent EPSC kinetic changes

Whereas jitter in the timing of vesicle release across individual release sites (inter-site synchrony) can contribute to the timing of EPSCs (Diamond and Jahr, 1995), MVR enables jitter between vesicle release events at a single site (intra-site synchrony). We found that activity dependent desynchronization requires MVR, such that under conditions of UVR increased CF stimulation no longer slowed the EPSC. Single-site desynchronization is further supported by low-affinity antagonist experiments that report a lower average glutamate concentration per site, not expected for inter-site asynchrony. Vesicle depletion during physiologically-relevant stimulation frequencies likely contributes to the reduced glutamate concentration per site (Dittman and Regehr, 1998; Foster and Regehr, 2004). However, depletion alone will speed the EPSC because the decay phase is dependent on the extent of MVR (Wadiche and Jahr, 2001). Our results support the idea that vesicle depletion contributes to frequency-dependent depression (Zucker and Regehr, 2002), but also highlight the role of vesicle release desynchronization. Although we cannot rule out the additional possibility that frequency-dependent desynchronization requires Ca^{2+} influx independent of MVR, the most parsimonious interpretation of our results is that activity

introduces jitter in the timing of the simultaneous release of multiple vesicles within single sites.

Mechanisms of activity-dependent MVR desynchronization

Repetitive activity can broaden the action potential due to K^+-channel inactivation, increasing calcium entry into the presynaptic terminal and leading to enhanced release (Geiger and Jonas, 2000). However, significant K^+-channel inactivation in our experiments is unlikely since the recovery time constant of fast-inactivating K-channels falls below our interstimulus interval of 0.5 s (Geiger and Jonas, 2000). In addition, the absence of frequency-dependent kinetic changes in 0.5 mM Ca^{2+} (Figure 2) suggests that action potential broadening does not occur under our conditions, since the typical action potential waveform is not sensitive to extracellular calcium (Isaacson and Walmsley, 1995; but see Schneggenburger et al., 1999). The requirement for extracellular Ca^{2+} also reduces the likelihood that mistiming of action potential propagation or invasion contributes to the slowing of the EPSC.

Rather, we speculate that 2 Hz stimulation affects presynaptic Ca^{2+} dynamics in a manner that impairs the simultaneous release of multiple vesicles per site. The precision and temporal spread of calcium domains between active zones or vesicle docking sites is assumed to dictate the synchrony of vesicle release. Repetitive stimulation may alter the temporal or spatial specificity of these domains as well as elevate residual calcium (Zucker and Regehr, 2002). We interpret the lack of activity-dependent desynchronization at 0.5 mM Ca^{2+} as evidence for the requirement of MVR. However, we cannot rule out that other direct or indirect calcium dependent processes contribute to desynchronization including the recruitment of spatially distant vesicles into the active readily releasable vesicle pool, inactivation of voltage-gated Ca^{2+} channels (Xu et al., 2007), calcium depletion from the synaptic cleft (Borst and Sakmann, 1999), or regulation of compound vesicle fusion (Singer et al., 2004; Matthews and Sterling, 2008; He et al., 2009). Future studies will explore these possibilities.

Purkinje cell complex spikes

CFs drive a distinctive high-frequency burst of spikes termed the complex spike (CpS; Eccles et al., 1966). The CpS waveform is subject to short- and long-term activity-dependent modulation during physiological relevant firing frequencies (Figure S2; Hashimoto and Kano, 1998; Hansel and Linden, 2000). Several mechanisms have been proposed to account for this activity-dependent regulation including presynaptic synaptic depression (Hashimoto and Kano, 1998), postsynaptic AMPAR occupancy (Foster et al., 2002), latent NMDA receptors (Piochon et al., 2007), use-dependent long-term plasticity (Weber et al., 2003), as well as regulation PC voltage-gated channel activity (Raman and Bean, 1997; Swensen and Bean, 2003; Zagha et al., 2008). We propose that desynchronization of MVR also contributes to activity-dependent alterations in the CpS. We found that the kinetics of the EPSC are slowed during physiological stimulation paradigms and these kinetic changes are both necessary (Figure 6) and sufficient (Figure 7) for alterations of the CpS waveform. Understanding how alterations in the timing of charge affect the conductances underlying the CpS will require further investigation.

Enhanced complex spike and calcium signaling during repetitive activity

CpSs are triggered at frequencies of 1 – 2 Hz *in vivo* (Armstrong and Rawson, 1979; Campbell and Hesslow, 1986). We found that desynchronized MVR during 2 Hz stimulation limits EPSC charge loss and alters the CpS waveform in a manner that favors successful spike propagation. Using dual somatic and axonal recordings we found that 2 Hz CF stimulation did, in fact, increase the probability of spikelet propagation even as the number

of somatic spikelets was reduced. Although our results suggest that activity-dependent desynchronization of MVR contributes to faithful spikelet propagation during physiological stimulation frequencies *in vitro*, the contribution of this mechanism to PC output *in vivo* requires further testing.

Regardless, alterations in spikelet propagation would enable activity-dependent CF regulation of PC output. First, because PCs release GABA onto neurons in deep cerebellar nuclei (DCN) at high frequency, the propagation probability of CpS spikelets is a critical determinant for IPSC timing. CpS spikelets propagate at ~150 – 375 Hz (Khaliq and Raman, 2005), allowing IPSCs to summate supra-linearly (Telgkamp and Raman, 2002). Hence, increased spikelet propagation probability will cause stronger inhibition of DCN neurons. Secondly, CF-activation pauses PC simple spikes for tens of milliseconds (Sato et al., 1992), allowing DCN neurons to depolarize and resume firing after hyperpolarization (Llinas and Muhlethaler, 1988; Aizenman et al., 1998) that can result in long term potentiation of inhibition at the PC-DCN synapse (Aizenman et al., 1998). Thus activity-dependent alteration in spikelet propagation can affect target neuron inhibitory summation and plasticity.

Kinetic changes in the CF-PC conductance will likely influence the amplitude and duration of dendritic calcium spikes, also enabling activity-dependent regulation of PC input. In addition to regulating the pause in firing that follows the CpS (Davie et al., 2008), dendritic calcium spikes are critical for synaptic plasticity. Correlated changes in the CpS shape and dendritic calcium signal have been reported following CF long-term plasticity (Weber et al., 2003). Hence, it is tempting to speculate that activity-dependent regulation of the CF-PC conductance modulates dendritic calcium transients as well as the pause of simple spikes to promote efficient inhibition onto DCN neurons. Taken together, desynchronization of MVR may have important implications for short-term synaptic integration, induction of plasticity, and motor learning.

Experimental Procedures

Tissue Preparation

Parasagittal cerebellar slices were prepared from postnatal day 13 – 22 mice (Harlan, Prattville, AL). The cerebellum was dissected out and glued to the stage of a vibroslicer (VT1200S, Leica Instruments, Bannockburn, IL), supported by a block of 4% agar. Dissection and cutting of slices was performed either in ice-cold solution containing (in mM) 75 NaCl, 2.5 KCl, 0.5 $CaCl_2$, 7 $MgCl_2$, 1.25 NaH_2PO_4, 26 $NaHCO_2$, 25 glucose, and 75 sucrose, or in ACSF (see below), bubbled with 95% O_2–5% CO_2. For axonal recordings animals were first perfused intracardially with an ice-cold solution containing (in mM) 110 choline chloride, 25 glucose, 25 $NaHCO_3$, 11.5 Na-ascorbate, 7 $MgCl_2$, 3 Na-pyruvate, 2.5 KCl, 1.25 NaH_2PO_4, 0.5 $CaCl_2$. Slices of 200 – 300 μm thickness were consecutively cut and incubated at 35°C for 30 min before use. All animal procedures were conducted in accordance with the National Institutes of Health Guide for the Care and Use of Laboratory Animals and with protocols approved by the local Institutional Animal Care and Use Committees.

During recordings, slices were superfused at a flow rate of 2 – 3 ml/minute with a solution containing (in mM) 125 NaCl, 2.5 KCl, 2.5 $CaCl_2$, 1.3 $MgCl_2$, 25 $NaHCO_2$, 1 NaH_2PO_4, 11 glucose, and 100 μM picrotoxin unless otherwise stated. In some experiments Ca^{2+} was reduced to 0.5 mM or 1 mM and Mg^{2+} was increased to 3.3 mM or 1 mM, respectively. Quantal-like, asynchronous events (Figure 5), were recorded by replacement of extracellular Ca^{2+} with 0.5 mM Sr^{2+} and increasing Mg^{2+} to 3.3 mM. To minimize voltage-clamp errors,

CF-PC EPSCs were either recorded between −65 mV and −70 mV in the presence of 600 – 800 nM NBQX or at depolarized potentials (−15 to −10 mV).

Drugs were applied in the bath- or via a flow pipe (ValveLink 8.2, Automate Scientific, Berkely, CA). Kynurenic acid (KYN) and NBQX were purchased from Ascent Scientific (Princeton, NJ), DL-*threo*-β-Benzyloxyaspartic acid (TBOA), cyclothiazide (CTZ), and (2S, 1′S,2′S)-2-(Carboxycyclopropyl) glycine (L-CCG-I) were purchased from Tocris Bioscience (Ellisville, MO). Picrotoxin was purchased from Sigma (St. Louis, MO).

Electrophysiology and Data Analysis

Whole-cell recordings were made from visually identified Purkinje cells (PCs) with a gradient contrast system using a 60X water-immersion objective on an upright microscope (Olympus BX51WI). Pipettes were pulled from either PG10165 glass (WPI, Sarasota, FL) with resistances of 0.8 – 1.5 MΩ or BF150–110 (Sutter Instruments, Novato, CA) with resistances of 1 – 1.5 MΩ. The series resistance (R_s), measured by the instantaneous current response to a 1 – 2 mV step with only the pipette capacitance cancelled, was < 5 MΩ (usually < 3 MΩ), and routinely compensated > 80%. Climbing fibers were stimulated (2 – 10 V, 20 – 200 μs) with a theta glass electrode (BT-150 glass, Sutter Instrument, Novato, CA) filled with extracellular solution placed in the granule cell layer. The paired-pulse ratio (PPR; 50 ms inter-stimulus interval) was determined following the stimulation train. Responses were recorded with a MultiClamp 700B amplifier (Molecular Devices, Sunnyvale, CA), filtered at 4 – 10 kHz and digitized (Digidata 1440A, Molecular Devices) at 50 – 100 kHz using Clampex 10 acquisition software (Molecular Devices). Pipette solutions for EPSC recordings contained (in mM) 35 CsF, 100 CsCl, 10 EGTA, and 10 HEPES, and 5 mM QX314, adjusted to pH 7.2 with CsOH or 9 mM KCl, 10 mM KOH, 120 mM K gluconate, 3.48 mM $MgCl_2$, 10 mM Hepes, 4 mM NaCl, 4 mM Na_2ATP, 0.4 mM Na_3GTP, and 17.5 mM sucrose (pH 7.25 with KOH) for current clamp recordings.

In current clamp recordings, PCs were injected with a negative current (< 500 pA) to maintain a membrane potential between − 65 and −70 mV during synaptic stimulation (−66.9 ± 0.8 mV at 0.05 Hz and −68.4 ± 0.8 mV at 2 Hz, n = 26; p > 0.05). The frequency of synaptic stimulation did not alter the CpS plateau potential from which spikelets were generated (−41.0 ± 0.9 mV at 0.05 Hz and −44.0 ± 1.1 mV at 2 Hz, n = 26; p > 0.05). For experiments described in Figure 7, the membrane potential was also kept at approximately −70 mV. The peak amplitude of the injected current used to evoke Cp-like-Ss varied across cells (range of 5 –18 nA that corresponds to peak conductances of 70 – 250 nS). The maximal rate of spikelet rise was measured from differentiating the complex spike waveform. Spikelets and their height were determined from trough-to-peak by setting the peak detection threshold to within 2 – 10% of the maximum peak with a separating valley of adjacent peaks of less than 90%. To calculate interspike intervals (ISIs), the time of spikelet peak amplitude was measured and subtracted from the peak time of the previous spikelet. All experiments were performed at 30° – 33°C attained with an inline heating device (Warner Instruments, Hamden, CT). Reported values are the mean ± SEM. Data was analyzed using AxographX (Axograph Scientific, Sydney, Australia), Microsoft Excel (Bellevue, WA), Prism, and InStat (GraphPad, La Jolla, CA). Statistical differences were assessed by two-tailed paired t-test unless otherwise noted and significance (denoted by figure asterisks) was assumed if $p < 0.05$. ANOVAs significance was determined with Dunnett's Multiple Comparison.

For axonal recordings, PCs with a visible axon (> 70 μm) were patched with an internal solution containing (in mM) 9 KCl, 10 KOH, 120 K-gluconate, 3.5 $MgCl_2$, 10 Hepes, 4 NaCl, 4 Na_2ATP, 0.4 Na_3GTP, 17.5 sucrose (pH 7.25) and 0.02 Alexa 594. After establishing whole-cell somatic recording, the PC was allowed to fill for 5 – 10 min and

axon identity was verified with 1 or 2 brief flashes of fluorescent light to minimize phototoxicity. A loose patch with a solution of (in mM) 145 NaCl, 10 HEPES (pH 7.25 with NaOH) was obtained at a distance of 202 ± 13 μm (range: 150 – 300 μm; n = 10) from the soma as measured with an eyepiece reticle. Somatic and axonal responses to CF stimulation were acquired at 100 kHz and digitally filtered at 10 kHz and 4 kHz, respectively. In some cases, axonal recordings were additionally filtered off-line at 2 – 3 kHz (Bessel filter) or with a 3 – 5 point boxcar filter (Axograph X). As in Khaliq and Raman (2005), we assessed axonal propagation success or failure by measuring the peak axonal response corresponding to a somatic spike and comparing with the baseline noise level. Briefly, somatic spikes were first identified with a threshold detection protocol. For each somatic spike, the time of peak was recorded, and the maximum value from the corresponding axonal trace was measured in a 1.5 ms time window centered on the somatic spike. Next, the baseline axonal recording noise was measured excluding intervals with corresponding somatic action potentials. The baseline axonal noise values were averaged to find the mean and SD. Axonal signals corresponding to somatic spikes were classified as successfully propagating spikelets if their amplitudes exceeded 4 SDs from the baseline noise. For each dual recording, somatic complex spikes were recorded and the axonal failures and successes were determined (from 54 ± 5 sweeps; range 17 - 103 sweeps) to obtain a probability of propagation for each spikelet. The cumulative propagation probability of at least 1, 2, 3, or 4 spikelets was calculated from the individual probabilities.

Supplementary Material

Refer to Web version on PubMed Central for supplementary material.

Acknowledgments

This work was supported by National Institutes of Health (NIH) Grant NS065920 and Boehringer Ingelheim Fonds (S.R.). We would like to thank Craig E. Jahr, Peter Jonas, Anastassios V. Tzingounis, and members of the Wadiche labs for discussions and critical reading of the manuscript.

References

Aizenman CD, Manis PB, Linden DJ. Polarity of long-term synaptic gain change is related to postsynaptic spike firing at a cerebellar inhibitory synapse. Neuron. 1998; 21:827–835. [PubMed: 9808468]

Armstrong DM, Rawson JA. Activity patterns of cerebellar cortical neurones and climbing fibre afferents in the awake cat. J Physiol (Lond). 1979; 289:425–448. [PubMed: 458677]

Atluri PP, Regehr WG. Delayed release of neurotransmitter from cerebellar granule cells. J Neurosci. 1998; 18:8214–8227. [PubMed: 9763467]

Auger C, Kondo S, Marty A. Multivesicular release at single functional synaptic sites in cerebellar stellate and basket cells. J Neurosci. 1998; 18:4532–4547. [PubMed: 9614230]

Barrett EF, Stevens CF. The kinetics of transmitter release at the frog neuromuscular junction. J Physiol (Lond). 1972; 227:691–708. [PubMed: 4405553]

Biró AA, Holderith NB, Nusser Z. Release probability-dependent scaling of the postsynaptic responses at single hippocampal GABAergic synapses. J Neurosci. 2006; 26:12487–12496. [PubMed: 17135411]

Borst JG. The low synaptic release probability in vivo. Trends Neurosci. 2010; 33:259–266. [PubMed: 20371122]

Borst JG, Sakmann B. Depletion of calcium in the synaptic cleft of a calyx-type synapse in the rat brainstem. J Physiol (Lond). 1999; 521(Pt 1):123–133. [PubMed: 10562339]

Boudkkazi S, Carlier E, Ankri N, Caillard O, Giraud P, Fronzaroli-Molinieres L, Debanne D. Release-dependent variations in synaptic latency: a putative code for short- and long-term synaptic dynamics. Neuron. 2007; 56:1048–1060. [PubMed: 18093526]

Campbell NC, Hesslow G. The secondary spikes of climbing fibre responses recorded from Purkinje cell axons in cat cerebellum. J Physiol (Lond). 1986; 377:225–235. [PubMed: 3795088]

Choi S, Klingauf J, Tsien RW. Postfusional regulation of cleft glutamate concentration during LTP at 'silent synapses'. Nat Neurosci. 2000; 3:330–336. [PubMed: 10725921]

Christie JM, Jahr CE. Multivesicular release at Schaffer collateral-CA1 hippocampal synapses. J Neurosci. 2006; 26:210–216. [PubMed: 16399689]

Clark BA, Monsivais P, Branco T, London M, Häusser M. The site of action potential initiation in cerebellar Purkinje neurons. Nat Neurosci. 2005; 8:137–139. [PubMed: 15665877]

Crowley JJ, Fioravante D, Regehr WG. Dynamics of fast and slow inhibition from cerebellar golgi cells allow flexible control of synaptic integration. Neuron. 2009; 63:843–853. [PubMed: 19778512]

Davie JT, Clark BA, Häusser M. The origin of the complex spike in cerebellar Purkinje cells. J Neurosci. 2008; 28:7599–7609. [PubMed: 18650337]

Diamond JS, Jahr CE. Asynchronous release of synaptic vesicles determines the time course of the AMPA receptor-mediated EPSC. Neuron. 1995; 15:1097–1107. [PubMed: 7576653]

DiGregorio DA, Nusser Z, Silver RA. Spillover of glutamate onto synaptic AMPA receptors enhances fast transmission at a cerebellar synapse. Neuron. 2002; 35:521–533. [PubMed: 12165473]

Dittman JS, Regehr WG. Calcium dependence and recovery kinetics of presynaptic depression at the climbing fiber to Purkinje cell synapse. J Neurosci. 1998; 18:6147–6162. [PubMed: 9698309]

Eccles JC, Llinás R, Sasaki K. The excitatory synaptic action of climbing fibres on the purinje cells of the cerebellum. J Physiol (Lond). 1966; 182:268–296. [PubMed: 5944665]

Fedchyshyn MJ, Wang LY. Activity-dependent changes in temporal components of neurotransmission at the juvenile mouse calyx of Held synapse. J Physiol. 2007; 581:581–602. [PubMed: 17347264]

Foster KA, Kreitzer AC, Regehr WG. Interaction of postsynaptic receptor saturation with presynaptic mechanisms produces a reliable synapse. Neuron. 2002; 36:1115–1126. [PubMed: 12495626]

Foster KA, Regehr WG. Variance-mean analysis in the presence of a rapid antagonist indicates vesicle depletion underlies depression at the climbing fiber synapse. Neuron. 2004; 43:119–131. [PubMed: 15233922]

Geiger JR, Jonas P. Dynamic control of presynaptic Ca(2+) inflow by fast-inactivating K(+) channels in hippocampal mossy fiber boutons. Neuron. 2000; 28:927–939. [PubMed: 11163277]

Goda Y, Stevens CF. Two components of transmitter release at a central synapse. Proc Natl Acad Sci USA. 1994; 91:12942–12946. [PubMed: 7809151]

Hansel C, Linden DJ. Long-term depression of the cerebellar climbing fiber--Purkinje neuron synapse. Neuron. 2000; 26:473–482. [PubMed: 10839365]

Harrison J, Jahr CE. Receptor occupancy limits synaptic depression at climbing fiber synapses. J Neurosci. 2003; 23:377–383. [PubMed: 12533597]

Hashimoto K, Kano M. Presynaptic origin of paired-pulse depression at climbing fibre-Purkinje cell synapses in the rat cerebellum. J Physiol (Lond). 1998; 506:391–405. [PubMed: 9490867]

He L, Xue L, Xu J, McNeil BD, Bai L, Melicoff E, Adachi R, Wu LG. Compound vesicle fusion increases quantal size and potentiates synaptic transmission. Nature. 2009; 459:93–97. [PubMed: 19279571]

Hefft S, Jonas P. Asynchronous GABA release generates long-lasting inhibition at a hippocampal interneuron-principal neuron synapse. Nat Neurosci. 2005; 8:1319–1328. [PubMed: 16158066]

Hestrin S, Nicoll RA, Perkel DJ, Sah P. Analysis of excitatory synaptic action in pyramidal cells using whole-cell recording from rat hippocampal slices. J Physiol (Lond). 1990; 422:203–225. [PubMed: 1972190]

Iremonger KJ, Bains JS. Integration of asynchronously released quanta prolongs the postsynaptic spike window. J Neurosci. 2007; 27:6684–6691. [PubMed: 17581955]

Isaacson JS, Walmsley B. Counting quanta: direct measurements of transmitter release at a central synapse. Neuron. 1995; 15:875–884. [PubMed: 7576636]

Katz B, Miledi R. The effect of temperature on the synaptic delay at the neuromuscular junction. J Physiol (Lond). 1965a; 181:656–670. [PubMed: 5880384]

Katz B, Miledi R. The measurement of synaptic delay, and the time course of acetylcholine release at the neuromuscular junction. Proc R Soc Lond, B, Biol Sci. 1965b; 161:483–495. [PubMed: 14278409]

Khaliq ZM, Raman IM. Axonal propagation of simple and complex spikes in cerebellar Purkinje neurons. J Neurosci. 2005; 25:454–463. [PubMed: 15647489]

Llinas R, Muhlethaler M. Electrophysiology of guinea-pig cerebellar nuclear cells in the in vitro brain stem-cerebellar preparation. J Physiol. 1988; 404:241–258. [PubMed: 2855348]

Lu T, Trussell LO. Inhibitory transmission mediated by asynchronous transmitter release. Neuron. 2000; 26:683–694. [PubMed: 10896163]

Maruta J, Hensbroek RA, Simpson JI. Intraburst and interburst signaling by climbing fibers. J Neurosci. 2007; 27:11263–11270. [PubMed: 17942720]

Matthews G, Sterling P. Evidence that vesicles undergo compound fusion on the synaptic ribbon. J Neurosci. 2008; 28:5403–5411. [PubMed: 18495874]

McKay BE, Molineux ML, Mehaffey WH, Turner RW. Kv1 K+ channels control Purkinje cell output to facilitate postsynaptic rebound discharge in deep cerebellar neurons. J Neurosci. 2005; 25:1481–1492. [PubMed: 15703402]

Monsivais P, Clark BA, Roth A, Häusser M. Determinants of action potential propagation in cerebellar Purkinje cell axons. J Neurosci. 2005; 25:464–472. [PubMed: 15647490]

Oertner TG, Sabatini BL, Nimchinsky EA, Svoboda K. Facilitation at single synapses probed with optical quantal analysis. Nat Neurosci. 2002; 5:657–664. [PubMed: 12055631]

Piochon C, Irinopoulou T, Brusciano D, Bailly Y, Mariani J, Levenes C. NMDA receptor contribution to the climbing fiber response in the adult mouse Purkinje cell. J Neurosci. 2007; 27:10797–10809. [PubMed: 17913913]

Prange O, Murphy TH. Analysis of multiquantal transmitter release from single cultured cortical neuron terminals. J Neurophysiol. 1999; 81:1810–1817. [PubMed: 10200215]

Raman IM, Bean BP. Resurgent sodium current and action potential formation in dissociated cerebellar Purkinje neurons. J Neurosci. 1997; 17:4517–4526. [PubMed: 9169512]

Sato Y, Miura A, Fushiki H, Kawasaki T. Short-term modulation of cerebellar Purkinje cell activity after spontaneous climbing fiber input. J Neurophysiol. 1992; 68:2051–2062. [PubMed: 1491256]

Scheuss V, Taschenberger H, Neher E. Kinetics of both synchronous and asynchronous quantal release during trains of action potential-evoked EPSCs at the rat calyx of Held. J Physiol (Lond). 2007; 585:361–381. [PubMed: 17916613]

Schmolesky MT, Weber JT, De Zeeuw CI, Hansel C. The making of a complex spike: ionic composition and plasticity. Ann N Y Acad Sci. 2002; 978:359–390. [PubMed: 12582067]

Schneggenburger R, Meyer AC, Neher E. Released fraction and total size of a pool of immediately available transmitter quanta at a calyx synapse. Neuron. 1999; 23:399–409. [PubMed: 10399944]

Singer JH, Lassová L, Vardi N, Diamond JS. Coordinated multivesicular release at a mammalian ribbon synapse. Nat Neurosci. 2004; 7:826–833. [PubMed: 15235608]

Sun J, Pang ZP, Qin D, Fahim AT, Adachi R, Südhof TC. A dual-Ca2+-sensor model for neurotransmitter release in a central synapse. Nature. 2007; 450:676–682. [PubMed: 18046404]

Swensen AM, Bean BP. Ionic mechanisms of burst firing in dissociated Purkinje neurons. J Neurosci. 2003; 23:9650–9663. [PubMed: 14573545]

Takahashi T, Forsythe ID, Tsujimoto T, Barnes-Davies M, Onodera K. Presynaptic calcium current modulation by a metabotropic glutamate receptor. Science. 1996; 274:594–597. [PubMed: 8849448]

Telgkamp P, Raman IM. Depression of inhibitory synaptic transmission between Purkinje cells and neurons of the cerebellar nuclei. J Neurosci. 2002; 22:8447–8457. [PubMed: 12351719]

Tong G, Jahr CE. Multivesicular release from excitatory synapses of cultured hippocampal neurons. Neuron. 1994; 12:51–59. [PubMed: 7507341]

Tzingounis AV, Wadiche JI. Glutamate transporters: confining runaway excitation by shaping synaptic transmission. Nat Rev Neurosci. 2007; 8:935–947. [PubMed: 17987031]

Vyshedskiy A, Allana T, Lin JW. Analysis of presynaptic Ca2+ influx and transmitter release kinetics during facilitation at the inhibitor of the crayfish neuromuscular junction. J Neurosci. 2000; 20:6326–6332. [PubMed: 10964937]

Wadiche JI, Jahr CE. Multivesicular release at climbing fiber-Purkinje cell synapses. Neuron. 2001; 32:301–313. [PubMed: 11683999]

Waldeck RF, Pereda A, Faber DS. Properties and plasticity of paired-pulse depression at a central synapse. J Neurosci. 2000; 20:5312–5320. [PubMed: 10884315]

Weber JT, De Zeeuw CI, Linden DJ, Hansel C. Long-term depression of climbing fiber-evoked calcium transients in Purkinje cell dendrites. Proc Natl Acad Sci USA. 2003; 100:2878–2883. [PubMed: 12601151]

Xu J, He L, Wu LG. Role of Ca(2+) channels in short-term synaptic plasticity. Curr Opin Neurobiol. 2007; 17:352–359. [PubMed: 17466513]

Xu-Friedman MA, Regehr WG. Probing fundamental aspects of synaptic transmission with strontium. J Neurosci. 2000; 20:4414–4422. [PubMed: 10844010]

Xu-Friedman MA, Regehr WG. Ultrastructural contributions to desensitization at cerebellar mossy fiber to granule cell synapses. J Neurosci. 2003; 23:2182–2192. [PubMed: 12657677]

Zagha E, Lang EJ, Rudy B. Kv3.3 channels at the Purkinje cell soma are necessary for generation of the classical complex spike waveform. J Neurosci. 2008; 28:1291–1300. [PubMed: 18256249]

Zucker RS, Regehr WG. Short-term synaptic plasticity. Annu Rev Physiol. 2002; 64:355–405. [PubMed: 11826273]

Highlights

1. Physiological frequency stimulation desynchronizes multivesicular release (MVR)
2. Desynchronized MVR slows the kinetics of EPSCs in the millisecond timescale
3. Desynchronized MVR alters the Purkinje cell complex spike (CpS) waveform
4. EPSC kinetics are necessary and sufficient to alter determinants of CpS propagation

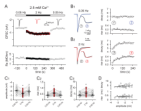

Figure 1. Time course and kinetics of CF-PC EPSCs at physiological firing frequencies

(A) Top: Time course of CF-PC EPSC peak amplitude evoked at 0.05 Hz (open circles) or at 2 Hz (red circles) in 2.5 mM external [Ca^{2+}]; (inset) averaged EPSCs during 0.05 Hz (black traces) and 2 Hz (red trace) CF stimulation. Bottom: Series resistance (open squares) for the EPSCs shown above.

(B1 and B2) Left: Superimposed EPSCs during 0.05 Hz (b1) and 2 Hz (b2) stimulation. Traces are the average of EPSCs at the beginning (black, *1* or *3*), during (grey), and at the end (blue or red, *2* or *3*) of a two minute stimulation period; (inset) rising phase of the normalized peak-amplitude EPSC in expanded time. Right: Time course of the decay time constant (circles) and rise time (squares) of EPSCs evoked with 0.05 Hz (top) or 2 Hz (bottom) stimulation. Linear regression (0.05 Hz) or a one-phase association curve (2 Hz) was used for line fits.

(C1 – C3) Summary data in 2.5 mM external Ca^{2+} shows the reduction of the EPSC peak amplitude (c1), the increase of the EPSC 20–80% rise time (c2), and decay time (c3) that occurs with 2 Hz CF-stimulation (red circles) compared to 0.05 Hz stimulation (open circles). Each data point represents an individual experiment, black horizontal traces are mean values ± SEM.

(D) No correlation between the kinetics and amplitude of 0.05 Hz stimulated EPSCs. Linear fit indicates no correlation between rise or decay time and EPSC peak amplitude (n = 30; p = 0.20 and 0.32 for the decay and the rise times, respectively).

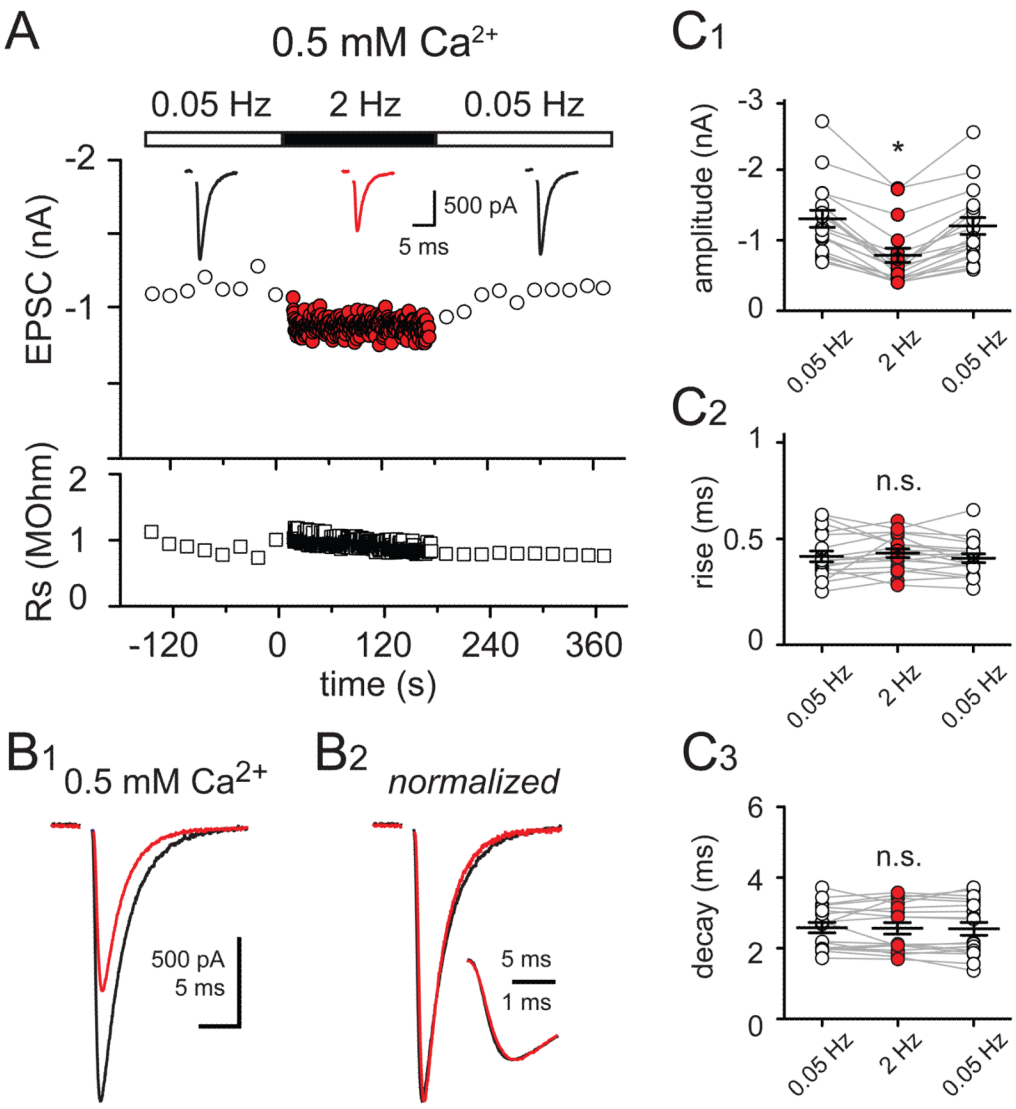

Figure 2. Kinetic changes during 2 Hz CF-stimulation require multivesicular release

(A) Top: Time course of CF-PC EPSC peak amplitude at 0.05 Hz (open circles) or 2 Hz (red circles) in 0.5 mM external Ca^{2+}; (inset) averaged EPSCs taken at the end of 0.05 Hz (black traces) and 2 Hz (red trace). Bottom: Time course of the series resistance (open squares) for the EPSCs shown above.

(B1) Superimposed averaged EPSCs evoked *after* two minutes of 0.05 Hz stimulation (black trace) or 2 Hz stimulation in 0.5 mM external [Ca^{2+}].

(B2) Responses in (B1) normalized to the peak amplitude; (inset) rising phases of the EPSCs in (B2) shown in expanded time.

(C1 – C3) Summary data of experiments performed in 0.5 mM external Ca^{2+} shows the reduction of the EPSC peak amplitude that occurs with 2 Hz CF stimulation (C1) but no change in the EPSC rise time (C2) or decay time (C3) with 2 Hz CF stimulation (red) compared to those during 0.05 Hz stimulation (open circles).

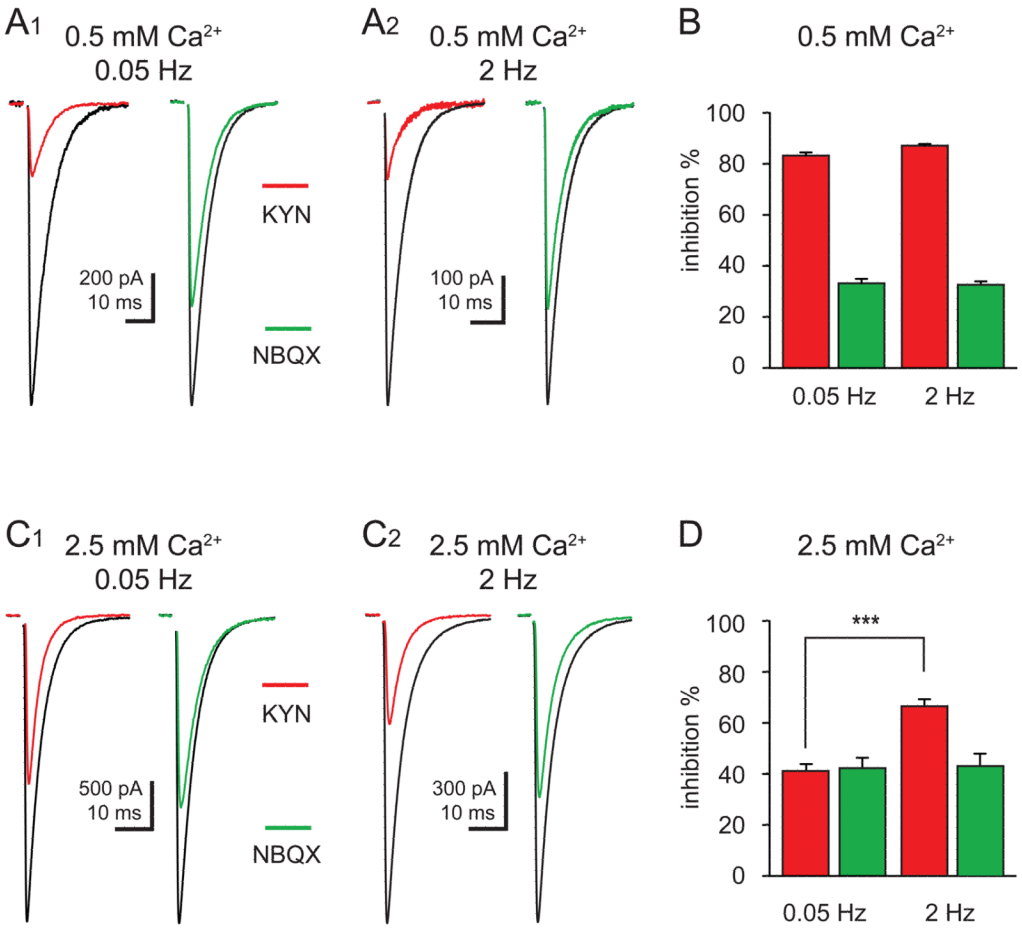

Figure 3. Activity-dependent inhibition of CF-PC EPSCs by a low affinity antagonist

(A1 and A2) Inhibition of CF-PC EPSCs (control; black) by 1 mM KYN (red) or 100 nM NBQX (green) recorded in 0.5 mM external Ca^{2+} at 0.05 Hz (A1) and 2 Hz (A2) stimulation frequency.

(B) Summary of EPSC inhibition by 1 mM KYN (red) or 100 nM NBQX (green) in 0.5 mM external Ca^{2+}.

(C1 and C2) Inhibition of CF-PC EPSCs in (control; black) by 1 mM KYN (red) or 100 nM NBQX (green) recorded in 2.5 mM external Ca^{2+} at 0.05 Hz (C1) and 2 Hz (C2) stimulation frequency.

(D) Summary of inhibition of EPSCs by 1 mM KYN (red) and 100 nM NBQX (green) in 2.5 mM external Ca^{2+}.

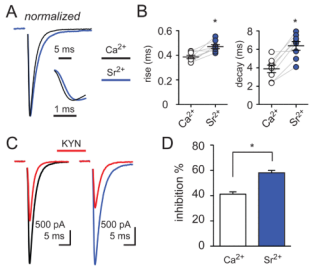

Figure 4. Strontium desynchronizes and reduces the peak synaptic [glutamate]

(A) Superimposed peak-scaled CF-PC EPSCs in Ca^{2+} (2 mM; black) and Sr^{2+} (5 mM; blue); (inset) rising phase of the EPSCs shown in expanded time.

(B) Summary data shows the increase in the rise (left) and decay (right) times of EPSCs in external Ca^{2+} (open circles; 0.38 ± 0.01 ms and 3.9 ± 0.41 ms, respectively) and Sr^{2+} (blue; 0.47 ± 0.02 and 6.4 ± 0.47 ms, respectively). Each data point represents individual experiments and black horizontal traces are mean values ± SEM.

(C) Superimposed CF-PC EPSCs in Ca^{2+} (left; black), in Sr^{2+} (right; blue), and the inhibition by 1 mM KYN (red) following 0.05 Hz stimulation.

(D) Summary of EPSC inhibition by 1 mM KYN in Ca^{2+} (open bar) and Sr^{2+} (blue).

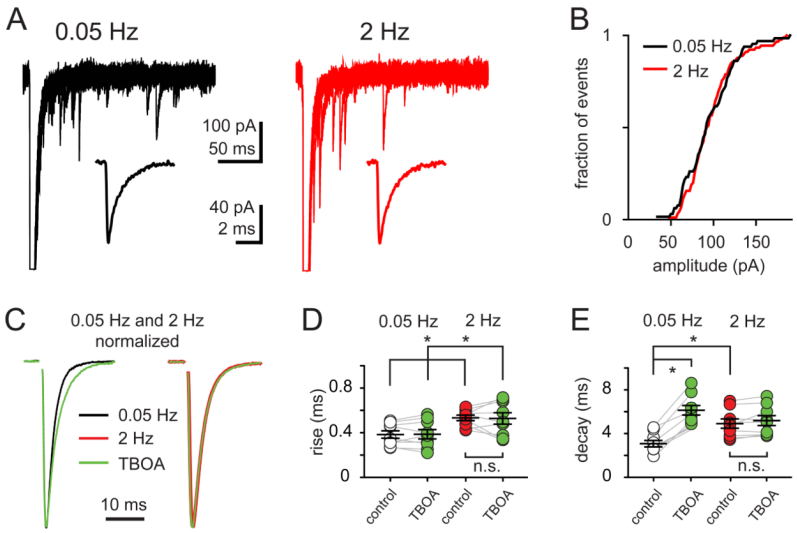

Figure 5. Activity-dependent EPSC kinetic changes are not due to decreased quantal size, altered quantal kinetics, or glutamate pooling

(A) Superimposed traces of aEPSCs in response to 0.05 Hz (A, black) and 2 Hz (B, red) stimulation in 0.5 mM Sr^{2+}; (insets) average aEPSCs collected from 50 – 100 stimuli delivered at each frequency. The rise (0.12 ± 0.07 ms versus 0.11 ± 0.05 ms) and decay times (1.44 ± 0.11 ms versus 1.41 ± 0.14 ms) at 0.05 Hz and 2 Hz, respectively, were not significantly different.

(B) Cumulative probability distribution of aEPSC amplitudes collected during 0.05 Hz (black) and 2 Hz (red) stimulation in 0.5 mM Sr^{2+} from a representative cell. Similar results were found in eleven cells tested.

(C) Superimposed peak-scaled 0.05 Hz- (left) and 2 Hz- (right) EPSCs in the absence (black) or in the presence of the glutamate transporter antagonist TBOA (50 μM, green).

(D and E) Summary data shows the rise (D), and decay times (E) of EPSCs evoked at 0.05 Hz or 2 Hz in the absence (open and red, respectively) or the presence of TBOA (50 μM; green). TBOA did not affect the rise time (0.38 ± 0.03 ms to 0.38 ± 0.04 ms) but prolonged the decay time of $EPSC_{0.05Hz}$ (from 3.8 ± 0.3 to 6.1 ± 0.4 ms in TBOA). TBOA neither changed the $EPSC_{2Hz}$ rise (0.53 ± 0.02 ms and 0.52 ± 0.05 ms) or decay (from 4.9 ± 0.4 ms and 5.1 ± 0.5 ms in TBOA) times.

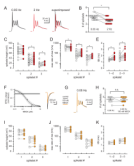

Figure 6. Frequency-dependent changes in Purkinje cell complex spikes are not due to synaptic depression

(A) Average complex spike (CpS) and superimposed individual responses (grey) evoked at 0.05 Hz (black) and 2 Hz (red). Superimposed averages (right) reveal loss and delay of spikelets during 2Hz stimulation.

(B) Summary data shows a reduction of the total number of spikelets during 2 Hz (red) compared to 0.05 Hz stimulation (open circles). Each data point represents individual experiments and black horizontal traces are the mean values ± SEM.

(C - E) Summary data of spikelet height (C), maximal spikelet rising rate (D), and inter-stimulus interval between spikelets (ISI; E) for the first three spikelets within CpSs evoked at 0.05 Hz (open circles) and 2 Hz (red).

(F) NBQX inhibition of EPSC. Grey horizontal bar denotes the 20–30% inhibition of charge. Solid line is a fit to the equation y = 1/(1+10^((Log$_{IC50}$ − x)*slope)) with an IC_{50} = 187 nM and slope of −1.2. Dashed lines represent the 95% confidence intervals of the fit. Right: Representative traces of the EPSC inhibition by 100 nM NBQX.

(G) Superimposed 0.05 Hz-stimulated CpSs in the absence (black) or presence of 100 nM NBQX (orange).

(H) Summary data of the total number of spikelets within CpSs at 0.05 Hz in the absence (open circles) and in the presence of 100 nM NBQX (orange). Only 1/10 cells tested lost a spikelet in NBQX.

(I – K) Summary of spikelet height (i; −2.5 ± 1.2%, −2.5 ± 1.5%, and 40.5 ± 19.0%; n = 10), maximal rate of spikelet rise (j; 0.2 ± 4.1%, 3.2 ± 11.9%, and 36.3 ± 17.8%; n = 10), and ISI (k; 3.3 ± 4.3%, 6.0 ± 5.3%; n = 9) of the first three spikelets within CpSs evoked at 0.05 Hz in the absence (open circles) and in the presence of 100 nM NBQX (orange). All values were not significantly different ($p \geq 0.05$; one sample t-test).

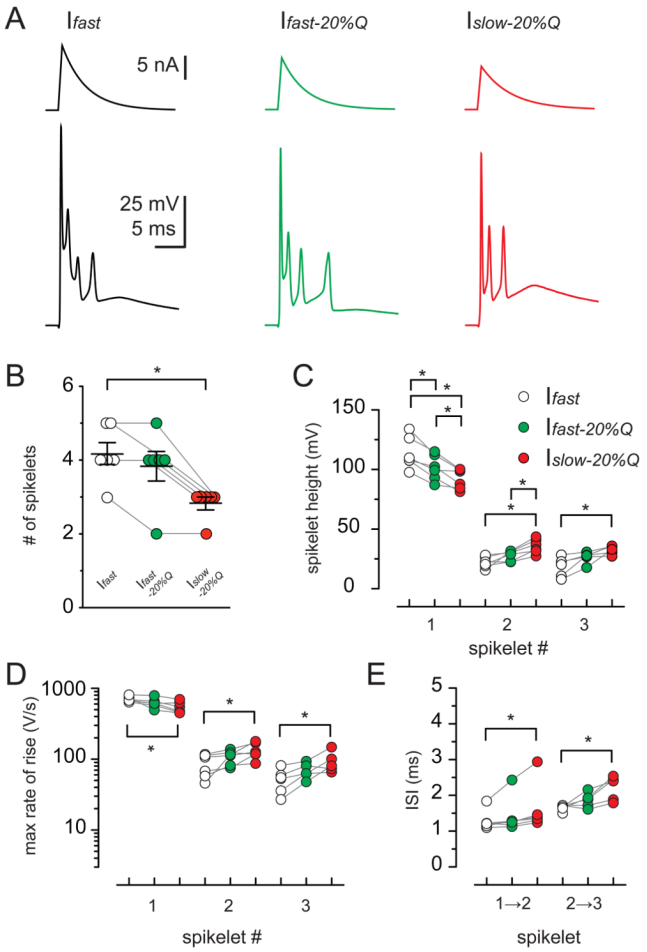

Figure 7. EPSC-like current injections mimic synaptic CF input

(A) PC complex-like-spikes (Cp-like-Ss; bottom) evoked by somatic current injection with fast kinetics (top traces; black; I_{fast}; 0.4 ms rise and 4 ms decay), fast kinetics with 80% charge of I_{fast} (green; $I_{fast\ -20\%Q}$), and slow kinetics with 80% charge of I_{fast} (red; $I_{slow-20\%Q}$; 0.4 ms rise and 5 ms decay).

(B) Summary data shows a reduction in the total number of spikelets as a result of $I_{slow-20\%Q}$ (red) current injection but not $I_{fast-20\%Q}$ (green) compared to I_{fast} (open circles; $p < 0.05$). Each data point represents individual experiments and black horizontal traces are the mean values ± SEM.

(C – E) Summary of spikelet height (C), maximal rate of spikelet rise (D), and ISI (E) of the first three spikelets within CpS evoked with I_{fast} (open circles), $I_{fast-20\%Q}$ (green), and $I_{slow-20\%Q}$ (red) current injection.

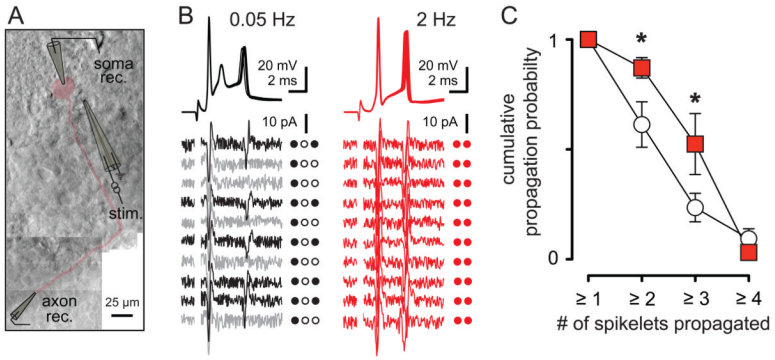

Figure 8. Stimulation frequency controls spikelet propagation probability

(A) Montage of dual somatic and axonal recording. The PC body and axon is highlighted in red. The recording (rec.) and stimulating (stim.) electrodes are traced for clarity.

(B) Ten superimposed somatically recorded CpSs (top) and corresponding axonal recordings (bottom) during CF stimulation at 0.05 Hz (black and grey) and 2 Hz (red). Black axonal traces indicate successes and grey traces indicate failures of spikelet propagation. Individual spike propagation success (filled circles) and failure (open circles) is also indicated to the right of each trace. Axonal recording site was estimated to be ~175 µm from soma.

(C) Summary data showing the probability of at least 'x' spikelets being propagated to the axonal recording site during 0.05 Hz (empty squares) or 2 Hz (red) stimulation.

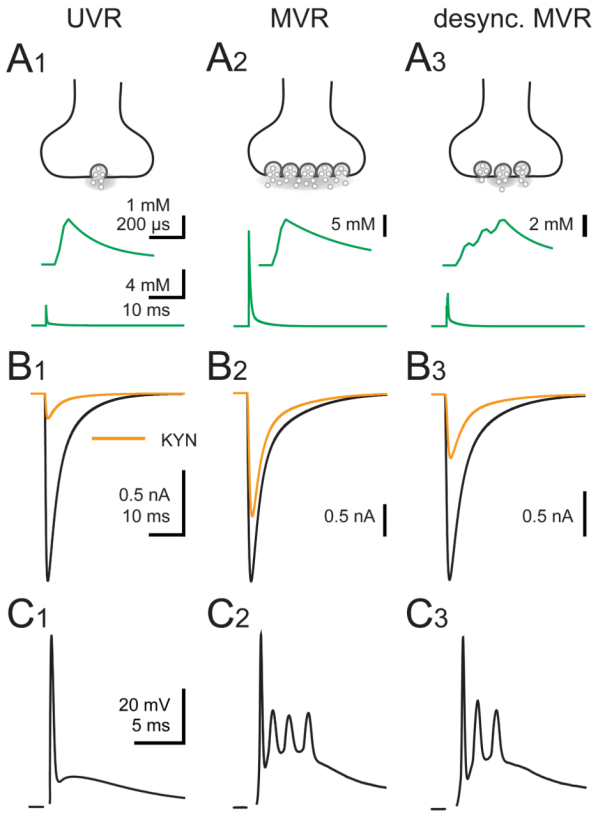

Figure 9. Numerical simulation of AMPA receptor EPSCs during UVR, MVR and desynchronized MVR

(A1 – A3) Cartoon representation (top) and glutamate transient (bottom; green) used to drive numerical simulations of an AMPAR model. In (A1), UVR was simulated with a peak [glutamate] transient of 2.4 mM that decays with two time constants (tau_{decay1} = 0.18 ms (84%) and tau_{decay2} = 3.4 ms). The [glutamate] transient used to simulate MVR (A2) has a peak amplitude of 12 mM that decays with time constants of 0.4 ms (86%) and 4.2 ms. Desynchronized MVR (desync.MVR; A3) was simulated from three linearly-summed UVR events offset by 100 µs. The peak [glutamate] reaches 4 mM. The 20–80% rise time for initial [glutamate] transient was set to 32 µs. Insets depict the [glutamate] transient in expanded scales for each release condition.

(B1 – B3) Simulated EPSCs (normalized) in the absence (black) and presence of 1 mM KYN (orange) driven by their respective glutamate transients (A1 – A3). See Supplementary information for rates.

(C1 – C3) CF-PC CpSs recorded in an extracellular solution containing either 0.5 mM Ca^{2+} (UVR; C1) or 2.5 mM Ca^{2+} at 0.05 Hz (MVR; C2) or 2 Hz (desync. MVR; C3).